

Suppression of viscosity enhancement around a Brownian particle in a near-critical binary fluid mixture

Youhei Fujitani[†]

School of Fundamental Science and Technology, Keio University, Yokohama 223-8522, Japan

(Received 23 March 2020; revised 5 August 2020; accepted 20 September 2020)

We consider the Brownian motion of a rigid spherical particle in a binary fluid mixture, which lies in the homogeneous phase near the demixing critical point, assuming that neither component is more attracted by the particle surface. In a recent study, it was experimentally shown that the self-diffusion coefficient first decreases and then reaches a plateau as the critical point is approached. The decrease should reflect the critical enhancement of the viscosity, while the plateau was interpreted as representing the suppression of the enhancement due to the shear around the particle. To examine this interpretation, we take into account the local shear rate to calculate the dependence of the drag coefficient on the particle speed, and then utilize a Langevin equation to calculate the self-diffusion coefficient.

Key words: colloids

1. Introduction

We consider the Brownian motion of a colloidal rigid particle in a binary fluid mixture lying in the homogeneous phase near the demixing critical point. In some combinations of the mixture and particle material, one of the components is preferentially attracted by the particle surface and the preferred component is remarkably adsorbed near the particle surface because of the near-criticality (Beysens & Leibler 1982; Beysens & Estève 1985). The particle motion deforms the adsorption layer, which affects the force exerted on the particle (Lee 1976; Omari, Grabowski & Mukhopadhyay 2009; Okamoto, Fujitani & Komura 2013; Fujitani 2018; Tani & Fujitani 2018; Yabunaka & Fujitani 2020). In other combinations exhibiting negligible preferential adsorption, the particle motion remains still influenced by the near-criticality because of the critical enhancement of the viscosity (Ohta 1975; Ohta & Kawasaki 1976). This enhancement can also be influenced by the particle motion, as is pointed out in a recent experimental work (Beysens 2019). We briefly mention its background in some paragraphs below.

Let us first assume there are no particles in an equilibrium near-critical binary fluid mixture. The composition can be represented by the difference between (or the ratio of) the mass densities of the two components. The order parameter, which we can take to be

[†] Email address for correspondence: youhei@appi.keio.ac.jp

proportional to the deviation of the local composition from the critical one, fluctuates about the equilibrium value on length scales smaller than the correlation length, ξ . Correlated clusters, where the order parameter keeps the same sign on average, range over these scales, and are convected to enhance the interdiffusion of the components on larger length scales (Kawasaki 1970; Onuki 2002). Thus, ξ affects how the two-time correlation function of the order-parameter fluctuation decays. Writing Γ_k for the relaxation coefficient of its spatial Fourier transform, with k denoting the magnitude of the wavenumber vector, we have

$$\Gamma_k = \Omega(k\xi) \times k^z, \quad (1.1)$$

for small k with $k\xi$ being finite. Here, z denotes the dynamic critical exponent for the order-parameter fluctuation and Ω represents a scaling function, which approaches a constant multiplied by $(k\xi)^{2-z}$ as $k\xi$ becomes much smaller than unity (Siggia, Hohenberg & Halperin 1976; Hohenberg & Halperin 1977). This leads to $\Gamma_k \propto k^2$ for sufficiently small k , which is expected for the hydrodynamic mode of a conserved quantity. We write k_B for the Boltzmann constant and T for the temperature of the mixture. The mode-coupling theory for a three-dimensional mixture gives

$$\Omega(k\xi) = \frac{k_B T}{6\pi\tilde{\eta}} \frac{K(k\xi)}{(k\xi)^3}, \quad (1.2)$$

where K denotes the Kawasaki function with $K(x) \approx 3\pi x^3/8$ for $x \gg 1$ and $K(x) \approx x^2$ for $x \ll 1$, and $\tilde{\eta}$ represents the shear viscosity (Kawasaki 1970; Onuki 2002). In this theory, the weak critical singularity of the viscosity is neglected, and the dynamic critical exponent is found to be three. This theoretical result turns out to be in good agreement with the experimental results (Swinney & Henry 1973). In the refined calculation of the dynamic renormalization group, the critical enhancement of $\tilde{\eta}$ is considered, and the value of z is found to be slightly larger than three (Folk & Moser 2006).

The mixture is assumed to be at equilibrium in the preceding paragraph. The critical enhancement of the transport coefficients, i.e. the Onsager coefficient for the interdiffusion and the shear viscosity, can be suppressed when a shear is imposed on the mixture. Influences of a simple shear flow are studied theoretically (Onuki & Kawasaki 1979; Onuki, Yamazaki & Kawasaki 1981) and experimentally (Beysens, Gbadamassi & Boyer 1979; Beysens & Gbadamassi 1980). In an example of this flow, the x component of the velocity is y multiplied by the constant shear rate s (> 0), with (x, y) denoting two of the three-dimensional Cartesian coordinates. A correlated cluster of the order-parameter fluctuation would be deformed by the shear when its lifetime is longer than a typical time scale of the shear, $1/s$. The lifetime for a cluster with the size of $1/k$ is evaluated to be $1/\Gamma_k$, while the cluster size ranges up to ξ . Hence, if the shear is strong enough to satisfy

$$s > \Gamma_{1/\xi}, \quad (1.3)$$

the enhancement is suppressed. This condition of strong shear is also derived in terms of the renormalization group, as mentioned in [appendix A](#).

A simple shear flow is a kind of linear shear flow, where the velocity \mathcal{V} at a position is proportional to the positional vector, and can be regarded as a linear combination of a stagnation-point flow and a purely rotational flow (Rallison 1984). These linear shear flows are two-dimensional. A pure-extension flow, being a three-dimensional linear shear flow, and a stagnation-point flow are referred to as elongational flows in Onuki & Kawasaki (1980*a,c*), where the suppression is studied for some linear shear flows. In a linear shear flow, the time derivative of a directed line segment X linking two fluid particles is equal

to $(\nabla V)^T \cdot X$, where the matrix ∇V represents the homogeneous velocity gradient and superscript T indicates the transposition. Thus, the exponential of the product of $(\nabla V)^T$ and the time t determines how X is stretched and shrunk with time. In the elongational flow, the shear rate s in (1.3) is given by the largest stretching rate, i.e. the largest eigenvalue of ∇V ; some details are mentioned in the penultimate paragraph of [appendix A](#).

The mean square displacement of a Brownian particle becomes proportional to the time interval as it becomes sufficiently long. The self-diffusion coefficient of the particle is defined as the constant of proportionality divided by twice the spatial dimension. In the study mentioned at the end of the first paragraph (Beysens 2019), it is shown that the self-diffusion coefficient of a Brownian particle in a near-critical binary fluid mixture first decreases and then reaches a plateau as T approaches the critical temperature T_c along the critical isochore in the homogeneous phase. The first decrease should reflect the critical enhancement of $\tilde{\eta}$, while the plateau can be regarded as representing the suppression of the enhancement due to the shear caused by the particle motion. Using (1.2) and replacing s in (1.3) with the average particle speed divided by the particle radius, Beysens (2019) estimates the temperature range exhibiting the suppression; the estimated range appears consistent with the observed one. In the present study, we calculate the self-diffusion coefficient for direct comparison with the experimental results.

In the first three subsections of § 2, we calculate the hydrodynamic force exerted on a rigid spherical particle moving translationally in a fluid mixture quiescent far from the particle. Assuming a typical length scale of the flow to be much larger than ξ , we need not consider dynamics of the order-parameter fluctuation, which is significant only on length scales smaller than ξ (Furukawa *et al.* 2013; Okamoto *et al.* 2013). The mixture is assumed to be incompressible, as in the previous studies mentioned above (Folk & Moser 1998; Onuki 2002). This assumption usually works well in a near-critical mixture prepared experimentally (Anisimov *et al.* 1995; Onuki 2002; Pérez-Sánchez *et al.* 2010). When the viscosity is homogeneous, the magnitude of the force is proportional to the particle speed. The constant of proportionality (the drag coefficient) is given by Stokes' law (Stokes 1851) and is linked with the self-diffusion coefficient of its Brownian motion through the Sutherland–Einstein relation (Einstein 1905; Sutherland 1905), although the Brownian motion is not always translational. This relation can be derived from the Langevin equation for the particle velocity (Bian, Kim & Karniadakis 2016), and is further founded on the fluctuating hydrodynamics (Bedeaux & Mazur 1974), even near the critical point (Mazur & van der Zwan 1978). In our problem, the suppression of the viscosity enhancement is locally determined by the inhomogeneous shear around the particle, and the drag coefficient can depend on the particle speed in its range to be considered in the Brownian motion. Neither Stokes' law nor the Sutherland–Einstein relation is applicable when the suppression occurs. Assuming the suppression to remain weak even if it is brought about by the local strong shear, we calculate the drag coefficient. In § 2.4, we use a one-dimensional Langevin equation to link the drag coefficient with the self-diffusion coefficient. Our results are shown and discussed in § 3, and summarized in § 4.

2. Formulation and calculation

We write d for the spatial dimension; our calculations in the text are limited to the case of $d = 3$. The values of the static critical exponents are shown in Pelissetto & Vicari (2002); we use $\nu \approx 0.630$ and $\eta \approx 0.0364$. The exponent η represents the deviation from the straightforward dimensional analysis of the static, or equal time, correlation function of the order-parameter fluctuation at the critical point. When the shear is not so strong as to suppress the critical enhancement, the correlation length ξ is homogeneously given

by $\xi = \xi_0 \tau^{-\nu}$ on the critical isochore, where τ is defined as $|T - T_c|/T_c$ and ξ_0 is a non-universal constant. Then, the singular part of the shear viscosity is proportional to $\tau^{\nu(d-z)}$ in a flow whose typical length is much larger than ξ , as described at (A 2). This exponent is measured to be around -0.042 (Berg & Moldover 1989, 1990), which leads to $z = 3.067$. Because $|\nu(d-z)|$ is small, the viscosity exhibits a very weak critical singularity. Thus, for the viscosity, the dependence of the regular part on τ is also significant unless the mixture is very close to the critical point, unlike for the Onsager coefficient of the interdiffusion. As in Beysens (2019), we use

$$\tilde{\eta}_B(T) \tau^{\nu(d-z)} \quad (2.1)$$

as the viscosity free from the shear effects. In this form of multiplicative anomaly, the regular part $\tilde{\eta}_B$ is defined as

$$\tilde{\eta}_B(T) = \tilde{\eta}_0 \exp\left(\frac{E_a}{k_B T}\right), \quad (2.2)$$

where $\tilde{\eta}_0$ is a non-universal constant and E_a denotes the activation energy (Sengers 1985; Mehrotra, Monnery & Svrcek 1996). Molecules would be required to overcome some energy barrier to shift their locations in a dense liquid. Equation (2.1) supposes $\tau < 1$ and the singular part represents the enhancement.

We define τ_s so that a given shear rate s affects the critical enhancement for $\tau < \tau_s$, and define s^* so that

$$\tau_s = \left(\frac{s}{s^*}\right)^{1/(\nu z)} \quad (2.3)$$

holds. Because of (1.1) and (1.3), s^* is independent of the imposed shear. We will later apply our results to a mixture of isobutyric acid and water. For this mixture under no shear, measured values of Γ_k/k^2 for small k in the neighbourhood of the critical point are shown in figure 10 of Chu, Schoenes & Kao (1968). These values and $\xi_0 = 0.3625$ nm (Beysens, Bourgou & Calmettes 1985) give $s^* = 3.7 \times 10^8$ s⁻¹ with the aid of (A 4) and (A 6).

From § 2.1 to § 2.3, we calculate the drag coefficient of a spherical rigid particle with radius r_0 , by assuming it to move translationally with the velocity $U\mathbf{e}_z$ in a binary fluid mixture in the absence of the preferential adsorption (figure 1). Here, \mathbf{e}_z denotes a unit vector. The mixture is on the critical isochore in the homogeneous phase with T being close to T_c , and is quiescent far from the particle. Assuming ξ to be much smaller than a typical length scale that the flow changes, we regard the local velocity field as a linear shear flow having the same velocity gradient to determine the local viscosity.

2.1. Assumption on the viscosity

We assume that the suppression of the critical enhancement of $\tilde{\eta}$ is perfect if it occurs, and thus the viscosity is assumed to be given by

$$\tilde{\eta} = \begin{cases} \tilde{\eta}_B(T) \tau^{\nu(d-z)} & \text{for } \tau > \tau_s, \\ \tilde{\eta}_B(T) \tau_s^{\nu(d-z)} & \text{for } \tau < \tau_s, \end{cases} \quad (2.4)$$

which supposes $\tau < 1$ and $\tau_s < 1$ because (2.1) underlies (2.4). This assumption is discussed in § 3. We write $\tilde{\eta}^{(0)}$ for (2.1), and define $\tilde{\eta}^{(1)}$ so that $\tilde{\eta} = \tilde{\eta}^{(0)} + \tilde{\eta}^{(1)}$ holds.

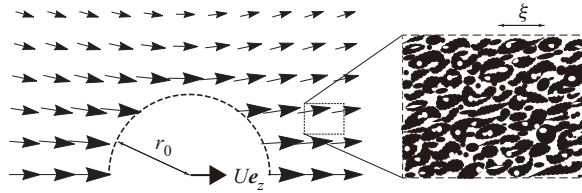


FIGURE 1. A drawing of a situation for our calculation of the drag coefficient from § 2.1 to § 2.3. A particle with the radius r_0 moves translationally with the velocity Ue_z in a mixture fluid quiescent far from the particle. A part of a cross-section containing the z axis is shown; the dashed curve represents half of the cross-section of the particle surface. The velocity field, represented by arrows outside the particle, is calculated with a homogeneous viscosity, although the viscosity becomes inhomogeneous when the suppression of the critical enhancement occurs somewhere. A magnified view of the smaller rectangular region is given in the larger one, where clusters are schematically drawn in black and white with some being deformed by the local shear. The correlation length ξ is assumed to be sufficiently small as compared with a typical length of the flow.

Introducing $\check{\tau}_s \equiv \tau_s/\tau$, we have

$$\tilde{\eta}^{(1)} \equiv \tilde{\eta}^{(0)} (\check{\tau}_s^{v(d-z)} - 1) \Theta(\check{\tau}_s - 1), \tag{2.5}$$

where Θ denotes the step function; $\Theta(x)$ vanishes for $x < 0$ and equals unity for $x > 0$. The shear rate is inhomogeneous, as shown later. Thus, the suppression makes the viscosity inhomogeneous. Subtracting the homogeneous part $\tilde{\eta}^{(0)}$ from the whole viscosity $\tilde{\eta}$ gives $\tilde{\eta}^{(1)}$, which is non-positive because of $d = 3 < z$.

The velocity and pressure fields, \mathbf{v} and p , satisfy the incompressibility condition and Stokes' equation, i.e.

$$\nabla \cdot \mathbf{v} = 0 \quad \text{and} \quad -\nabla p + 2\nabla \cdot (\tilde{\eta}\mathbf{E}) = 0, \tag{2.6a,b}$$

where \mathbf{E} is the rate-of-strain tensor. Here, a low Reynolds number is assumed, as discussed in § 2 of Yabunaka & Fujitani (2020). The no-slip boundary condition is imposed at the particle surface, while \mathbf{v} tends to zero and p approaches a constant, denoted by p_∞ , far from the particle.

2.2. Approximation for a weak suppression

We consider a particular time and take the spherical coordinates (r, θ, ϕ) so that the origin is at the particle's centre and that the polar axis (z axis) is along e_z ; the coordinate z should not be confused with the dynamic critical exponent. The unit vectors in the directions of r and θ are denoted by e_r and e_θ , respectively. The no-slip condition gives $\mathbf{v} = Ue_z$ at $\rho = 1$, where ρ denotes a dimensionless radial distance, r/r_0 . We can assume $v_\phi = 0$. The drag force is along the z axis; its z component, denoted by \mathcal{F}_z , is given by the surface integral of $(2\tilde{\eta}\mathbf{E} \cdot e_r - pe_r) \cdot e_z$ over the particle surface. The drag coefficient is given by $-\mathcal{F}_z/U$, and can depend on U in our problem. Thus, we write $\gamma(U)$ for the drag coefficient.

We, respectively, write $\mathbf{v}^{(0)}$ and $p^{(0)}$ for the velocity and pressure fields obtained when the viscosity is forced to be $\tilde{\eta}^{(0)}$ homogeneously. Equation (2.6a,b) yields

$$\nabla \cdot \mathbf{v}^{(0)} = 0 \quad \text{and} \quad -\nabla p^{(0)} + \tilde{\eta}^{(0)} \Delta \mathbf{v}^{(0)} = 0. \tag{2.7a,b}$$

The boundary conditions are $\mathbf{v}^{(0)} = U\mathbf{e}_z$ at $\rho = 1$, and $\mathbf{v}^{(0)} \rightarrow \mathbf{0}$ and $p^{(0)} \rightarrow p_\infty$ as $\rho \rightarrow \infty$. The solution is well known (Stokes 1851) and is given by

$$p^{(0)} = p_\infty + \frac{3\tilde{\eta}^{(0)}}{2r_0\rho^2}U \cos \theta, \quad v_r^{(0)} = \frac{3\rho^2 - 1}{2\rho^3}U \cos \theta, \quad v_\theta^{(0)} = -\frac{3\rho^2 + 1}{4\rho^3}U \sin \theta \tag{2.8a-c}$$

and $v_\phi^{(0)} = 0$. The arrows outside the particle in figure 1 represent $\mathbf{v}^{(0)}$ for $U > 0$. The superscript (0) is also added to a quantity calculated from $\mathbf{v}^{(0)}$ and $p^{(0)}$. The drag coefficient calculated from (2.8a-c) is given by

$$\gamma^{(0)} = -\frac{\mathcal{F}_z^{(0)}}{U} = 6\pi\tilde{\eta}^{(0)}r_0, \tag{2.9}$$

which is independent of U and represents Stokes' law. We define $\mathbf{v}^{(1)}$ and $p^{(1)}$ as $\mathbf{v} - \mathbf{v}^{(0)}$ and $p - p^{(0)}$, respectively. They satisfy $\nabla \cdot \mathbf{v}^{(1)} = 0$ and

$$-\nabla p^{(1)} + \tilde{\eta}^{(0)} \Delta \mathbf{v}^{(1)} = -2\nabla \cdot (\tilde{\eta}^{(1)} \mathbf{E}). \tag{2.10}$$

The boundary conditions are

$$\left. \begin{aligned} \mathbf{v}^{(1)} &= \mathbf{0} \quad \text{at } \rho = 1 \quad \text{and} \\ \mathbf{v}^{(1)} &\rightarrow \mathbf{0} \quad \text{and} \quad p^{(1)} \rightarrow 0 \quad \text{as } \rho \rightarrow \infty. \end{aligned} \right\} \tag{2.11}$$

In the flow field of \mathbf{v} and p , we define κ as the maximum value of a dimensionless ratio $|\tilde{\eta}^{(1)}/\tilde{\eta}^{(0)}|$. Equation (2.5) is proportional to κ . From (2.10) and (2.11), $\mathbf{v}^{(1)}$ is also proportional to κ . The particle speed supposed here lies in the range involved in the Brownian motion. We assume that τ is not so small as to cause strong suppression, and assume κ to be so small that the calculation up to the order of κ makes sense. At this order, (2.10) becomes

$$-\nabla p^{(1)} + \tilde{\eta}^{(0)} \Delta \mathbf{v}^{(1)} = -\tilde{\eta}^{(1)} \Delta \mathbf{v}^{(0)} - (2\nabla \tilde{\eta}^{(1)}) \cdot \mathbf{E}^{(0)}. \tag{2.12}$$

Here, s contained in $\tilde{\eta}^{(1)}$ is replaced by $s^{(0)}$, which is the shear rate calculated from $\mathbf{v}^{(0)}$. Likewise, we can evaluate κ by using $s^{(0)}$ instead of s in (2.5). We define $\mathcal{F}_z^{(1)}$ so that $\mathcal{F}_z = \mathcal{F}_z^{(0)} + \mathcal{F}_z^{(1)}$ holds. At the order of κ , $\mathcal{F}_z^{(1)}$ equals the surface integral of

$$2\tilde{\eta}^{(1)} \mathbf{E}_{rz}^{(0)} + 2\tilde{\eta}^{(0)} \mathbf{E}_{rz}^{(1)} - p^{(1)} \mathbf{e}_r \cdot \mathbf{e}_z \tag{2.13}$$

over the particle surface, where $\mathbf{E}^{(1)}$ is the rate-of-strain tensor for $\mathbf{v}^{(1)}$ and $p^{(1)}$.

On the z axis, the components of $\nabla \mathbf{v}^{(0)}$ with respect to the Cartesian coordinates (x, y, z) is expressed by $\partial_z v_z^{(0)}$ multiplied by a traceless diagonal matrix, whose diagonal elements are $-1/2, -1/2$ and 1 from the top. Here, ∂_z indicates the partial derivative with respect to z . Thus, noting the description at the end of the preface of § 2, we can regard $\mathbf{v}^{(0)}$ on the z axis as a pure-extension flow locally. In particular, at a point with $\theta = \pi$ for $U > 0$,

the largest stretching rate occurs in the z direction, i.e. the radial direction, and is given by $\partial_r v_r^{(0)}$. As θ approaches $\pi/2$, periodic motion becomes predominant over elongational motion in $\mathbf{v}^{(0)}$, as is suggested by figure 1 and is explicitly shown in appendix B. A rotational flow is found to be weak in suppressing the critical enhancement (Onuki & Kawasaki 1980c). Thus, considering the discussion on the elongational flow in the fourth paragraph of § 1, we assume that $s^{(0)}$ is given by the largest real-part of the eigenvalues of $\nabla \mathbf{v}^{(0)}$. Calculating them directly from (2.8a–c), we find $s^{(0)}$ to be given by

$$s^{(0)}(\rho, \theta) = \left| \frac{3cU}{4r_0} \left(\frac{1}{\rho^2} - \frac{1}{\rho^4} \right) \cos \theta \right|, \tag{2.14}$$

where a positive factor c , depending on θ , ranges from $1/2$ to 2 . Equation (2.14) with $c = 2$ equals $|\partial_r v_r^{(0)}|$. We proceed below with calculations by regarding c as a constant, in spite of the actual dependence of c on θ . It will be shown later that our result of the self-diffusion coefficient is rather insensitive to the value of c .

2.3. Expansions with respect to the spherical harmonics

The flow we consider here is symmetric with respect to the polar axis, and thus the angular part of $\mathbf{v}^{(1)}$ can be expanded in terms of the vector spherical harmonics,

$$\mathbf{P}_{J0} = Y_{J0} \mathbf{e}_r \quad \text{and} \quad \mathbf{B}_{J0} = \frac{r \nabla Y_{J0}}{\sqrt{J(J+1)}} \tag{2.15a,b}$$

for $J = 1, 2, \dots$ (Morse & Feshbach 1953; Barrera, Estévez & Giraldo 1985; Fujitani 2007). Here, $Y_{J0}(\theta)$ is one of the spherical harmonics, $\sqrt{(2J+1)/(4\pi)} P_J(\cos \theta)$, with P_J denoting the Legendre polynomial, e.g. $P_1(x) = x$. The mode $J = 0$ need not be considered because of the incompressibility. We define functions Π_J, R_J and T_J so that

$$p^{(1)} = \sum_J \Pi_J(\rho) Y_{J0}(\theta) \quad \text{and} \quad \mathbf{v}^{(1)} = \sum_J [R_J(\rho) \mathbf{P}_{J0}(\theta, \phi) + T_J(\rho) \mathbf{B}_{J0}(\theta, \phi)] \tag{2.16a,b}$$

hold. We expand the negative of the right-hand side of (2.12) as

$$\sum_J [F_J(\rho) \mathbf{P}_{J0}(\theta, \phi) + H_J(\rho) \mathbf{B}_{J0}(\theta, \phi)], \tag{2.17}$$

whereby F_J and H_J are defined. They are obtained with the aid of the orthogonality of the vector spherical harmonics. The incompressibility condition gives

$$T_J(\rho) = \frac{1}{\rho \sqrt{J(J+1)}} \partial_\rho \rho^2 R_J(\rho). \tag{2.18}$$

We use (2.18) to delete T_J from the r and θ components of (2.12), which are combined to give

$$(\rho \partial_\rho + J) (\rho \partial_\rho + J + 2) (\rho \partial_\rho - J + 1) (\rho \partial_\rho - J - 1) R_J(\rho) = -X_J(\rho). \tag{2.19}$$

Here, X_J is defined as

$$X_J(\rho) = \frac{r_0^2 \rho^2}{\tilde{\eta}^{(0)}} \left[\sqrt{J(J+1)} \partial_\rho \rho H_J(\rho) - J(J+1) F_J(\rho) \right]. \tag{2.20}$$

Similar calculations can be found in deriving (2.17) of Fujitani (2007) and in deriving (3.20) of Yabunaka & Fujitani (2020). Equations (2.11) and (2.18) give

$$R_J(\rho) = \partial_\rho R_J(\rho) = 0 \quad \text{at } \rho = 1 \quad \text{and} \quad R_J(\rho) \rightarrow 0 \quad \text{as } \rho \rightarrow \infty. \tag{2.21}$$

Applying the method of variation of parameters, we can rewrite (2.19) as

$$R_J(\rho) = \int_1^\infty d\sigma \Gamma_J(\rho, \sigma) X_J(\sigma), \tag{2.22}$$

where the kernel Γ_J is given in appendix C.

The first term of (2.13) does not contribute to $\mathcal{F}_z^{(1)}$ because (2.14), and thus (2.5), vanish at the particle surface. With the aid of (2.18), we use the θ component of (2.12) to delete Π_J and T_J from the last two terms of (2.13). These terms are thus rewritten as the sum of terms involving R_J and H_J over J . Only the terms involving R_1 are left after the surface integration of (2.13), as shown by (C 4) and described below (C 5). Substituting (2.22) into the result of the surface integration, we use

$$\left(\frac{1}{2}\partial_\rho^3 + 2\partial_\rho^2\right) \Gamma_1(\rho, \sigma) = \frac{3\sigma^2 - 1}{4\sigma^3} \quad \text{at } \rho = 1. \tag{2.23}$$

The right-hand side above is related to the fraction appearing in (2.8b) because of the Lorentz reciprocal theorem (Lorentz 1896), as shown in appendix B of Fujitani (2018) and mentioned at (A2) of Yabunaka & Fujitani (2020). We thus arrive at

$$\mathcal{F}_z^{(1)} = \mathcal{F}_z^{(0)} \int_1^\infty d\rho \frac{3\rho^2 - 1}{\rho^3} \check{X}(\rho), \tag{2.24}$$

where \check{X} is defined as

$$\check{X}(\rho) \equiv \sqrt{\frac{3}{\pi}} \frac{X_1(\rho)}{36U}. \tag{2.25}$$

As shown by (C 7), \check{X} is given in terms of the integral with respect to θ because (2.20) involves F_1 and H_1 , which are calculated from the right-hand side of (2.12) with the aid of the orthogonality of the vector spherical harmonics. Thus, (2.24) contains a double integral with respect to ρ and θ . We have analytical results for the integrals with respect to ρ , as described at the end of appendix C, and thus what to calculate numerically is the integration with respect to θ .

We find \check{X} to depend on U only through $\tau_{s^{(0)}}$. With U^* denoting s^*r_0 , the ratio $\gamma(U)/\gamma^{(0)} = 1 + (\mathcal{F}_z^{(1)}/\mathcal{F}_z^{(0)})$ is a function of a dimensionless speed $|U|/U^*$ because of (2.3) and (2.14), and is denoted by $\check{\gamma}(U/U^*)$. Using the value of the critical exponents stated in the preface of § 2, we numerically calculate the integral of (2.24) to obtain $\check{\gamma}(u)$. In figure 2, $\check{\gamma}(u)$ decreases as u increases, which represents that the critical enhancement of $\tilde{\eta}$ is suppressed more as the faster particle causes stronger shear. At the smaller value of τ , the suppression is shown to be stronger, which can be explained by the existence of larger clusters deformable for smaller u .

2.4. Description of the Brownian motion

When the viscosity is homogeneous in the absence of the suppression, as mentioned in § 1, a simple description of the Brownian motion is given by the Langevin equation for

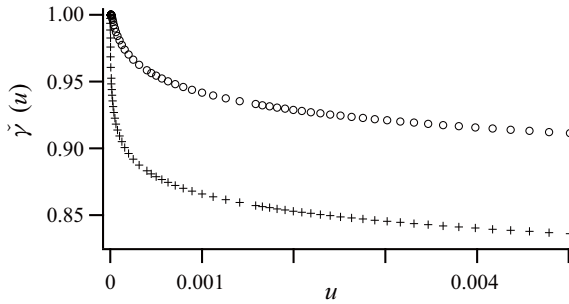


FIGURE 2. We plot $\check{\gamma}(u)$ for $\tau = 1.008 \times 10^{-3}$ (o) and 1.26×10^{-4} (+). As mentioned in the text, $\check{\gamma}$ represents the drag coefficient non-dimensionalized by (2.9), while u represents the particle speed non-dimensionalized by $U^* \equiv s^*r_0$.

the particle velocity, where the force exerted on the particle is separated into the thermal noise and the instantaneous friction force (Bian *et al.* 2016). The former represents the force varying much more rapidly than the latter and vanishes after being averaged over a macroscopic time interval (Sekimoto 2010), while the friction coefficient in the latter equals the drag coefficient given by Stokes’ law. This is founded in terms of the fluctuating hydrodynamics (Bedeaux & Mazur 1974; Mazur & van der Zwan 1978) and is numerically verified (Kebblinski & Thomin 2006). The components of the thermal noise in the three orthogonal directions are statistically independent, and thus the self-diffusion coefficient can be calculated in one dimension. To calculate the self-diffusion coefficient in our problem, we still use the drag coefficient $\gamma(U)$ as the friction coefficient in the Langevin equation, considering that the viscosity can be only weakly inhomogeneous depending on the particle speed. This amounts to assuming $\gamma(U)$ to be most probable friction coefficient when the particle velocity is U in the Brownian motion at the time resolution of the Langevin equation.

The effective mass, denoted by m , is the sum of the particle mass and half the mass of the displaced fluid (Lamb 1932; Bian *et al.* 2016; Fujitani 2018). Here, unlike in the preceding subsections, U is a stochastic variable depending on the time t . The Langevin equation is

$$m \frac{dU}{dt} = -\gamma(U)U + b(U) \circ \frac{dW}{dt}, \tag{2.26}$$

where W represents the Wiener process and the symbol \circ indicates that (2.26) should be interpreted in the Stratonovich sense (Risken 2002; Sekimoto 2010). The positive function $b(U)$ is fixed so that (2.26) is consistent with the Boltzmann distribution, as shown in appendix D. The self-diffusion coefficient of the particle D is given by (Bian *et al.* 2016)

$$D = \int_0^\infty dt \langle U(t)U(0) \rangle, \tag{2.27}$$

where $\langle \dots \rangle$ means the equilibrium average. Defining M as $mU^{*2}/(k_B T)$, we utilize the Laplace transformation to obtain

$$D = \frac{k_B T}{\gamma^{(0)}} \sqrt{\frac{1}{2\pi M}} \int_0^\infty du \left[\int_u^\infty du_1 \check{\gamma}(u_1) u_1 e^{-Mu_1^2} \right]^{-1} e^{-3Mu^2/2}, \tag{2.28}$$

as shown in appendix D. This equation can be also derived from (2.26) by using not the Laplace transformation but some of the equations in § S.9 of Risken (2002). Converting the

integration variables u and u_1 to $u\sqrt{M}$ and $u_1\sqrt{M}$, respectively, we find that D depends on M only through the variable of $\check{\gamma}$.

Equation (2.28) involves $\check{\gamma}(u)$ for infinitely large u because (2.26) formally supposes any particle speed, including the particle speed larger than assumed in the hydrodynamic formulation. This is also the case with the Langevin equation supposing a constant drag coefficient, where Stokes' law is assumed even for particle speeds so large as to break the validity of the Stokes approximation. In either case, we can avoid this inconvenience in computing the self-diffusion coefficient, to which such large speed never contributes. An effective cutoff speed is implicitly imposed on the Langevin equation. This point is discussed in the next section.

3. Results and discussion

Latex beads with radius 80 nm are put in a mixture of isobutyric acid and water in the experiment of Beysens (2019), where we have $m = 3.32 \times 10^{-18}$ kg and $U^* = 29.6$ m s⁻¹. The mixture can be regarded as incompressible near the demixing critical point (Clerke & Sengers 1983; Onuki 2002). The thermal average of U is 3.53×10^{-2} m s⁻¹, which is denoted by \bar{U} . The improper integrals in (2.28) can be replaced by definite integrals involving only particle speeds smaller than approximately $4\bar{U}$, as described in the latter half of appendix D. Because the viscosity of the mixture is around 2.5×10^{-3} kg m⁻¹ s⁻¹ (Allegra, Stein & Allen 1971), the Reynolds number is 1.4×10^{-2} for $U = \bar{U}$, and remains sufficiently small as compared with unity even if multiplied by four. This is consistent with our hydrodynamic formulation. The variable u in figure 2 represents U/U^* , which equals 1.19×10^{-3} for $U = \bar{U}$. Thus, the range of the horizontal axis in figure 2 approximately coincides with the integration interval of the definite integrals used in our numerical calculation.

The data of the self-diffusion coefficient in Beysens (2019), ranging over $6.31 \times 10^{-5} \leq \tau \leq 6.81 \times 10^{-2}$, are replotted with open circles in figure 3. The viscosity of the near-critical mixture of isobutyric acid and water, containing no particles, is measured in Allegra *et al.* (1971). From the data in their table 2, with the ones for four values of τ from the smallest being excluded according to Oxtoby (1975), we calculate the self-diffusion coefficient by applying Stokes' law and the Sutherland–Einstein relation, i.e. by dividing $k_B T / (6\pi r_0)$ by the viscosity, and plot the results with crosses in figure 3. The crosses, ranging over $1.14 \times 10^{-4} \leq \tau \leq 2.78 \times 10^{-2}$, agree with the open circles for $\tau > 7 \times 10^{-3}$. These open circles and the crosses should be explained by using (2.1), i.e. $\tilde{\eta}^{(0)}$, which is free from the suppression due to the shear.

Conversely, we can calculate the viscosity from the open circles for $\tau > 7 \times 10^{-3}$ by applying Stokes' law and the Sutherland–Einstein relation. In a graph (not shown here) where these results and the data of Allegra *et al.* (1971) with the exclusion above are linearly plotted against τ , we perform the curve-fit to $\tilde{\eta}^{(0)}$ with the aid of 'NonlinearModelFit' of Mathematica (Wolfram Research) by using $T_c = 300.1$ K (Toumi & Bouanz 2008) and the values of the critical exponents stated in the preface of § 2. Estimated values are $\tilde{\eta}_0 = 3.38 \times 10^{-6}$ kg m s⁻¹ and $E_a / (k_B T_c) = 6.35$ with the standard deviations being 5.11×10^{-7} kg m s⁻¹ and 1.53×10^{-1} , respectively. We use the estimated values to calculate $\tilde{\gamma}^{(0)} = 6\pi\tilde{\eta}^{(0)}r_0$ and plot $k_B T / \gamma^{(0)}$ with the dashed curve in figure 3; the curve agrees well with the data applied to the curve-fit. Employing $\tilde{\gamma}^{(0)}$ thus obtained, we calculate the prefactor of (2.28), whose integrals are numerically calculated after being replaced by the definite integrals mentioned above. Our results of D for $c = 1$ are plotted with solid circles in figure 3. It appears that the open circles saturate to reach a plateau as

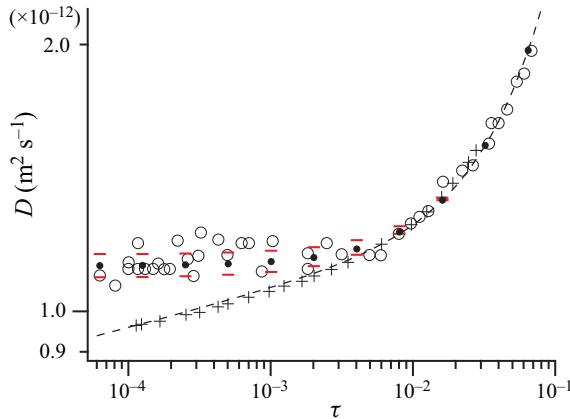


FIGURE 3. Plot of the self-diffusion coefficient against τ . Open circles represent the experimental data of Beysens (2019), where T_c is estimated to be 301.1 K. Crosses come from Allegra *et al.* (1971), with T_c being estimated to be 299.4 K. The dashed curve represents $k_B T / (6\pi\tilde{\eta}^{(0)}r_0)$, which we calculate by using the parameter values estimated from the open circles for $\tau > 7 \times 10^{-3}$ and the crosses. Solid circles represent our results of (2.28) for $c = 1$. The red short bar above (below) each of the solid circles for $\tau \leq 1.61 \times 10^{-2}$ represents (2.28) for $c = 4$ (0.25).

τ decreases below 3.2×10^{-3} , although they are distributed rather widely in the direction of the vertical axis. Our results pass through the middle of the distribution. This strongly suggests that the saturation should represent the suppression of the critical enhancement of $\tilde{\eta}$ due to the local shear caused by the particle motion, as claimed by Beysens (2019).

Figure 4 shows that our calculation results of D increase as c increases, which can be expected because the shear is then evaluated to be larger. In this figure, the ratios of the change in D lie within 5% when c changes from unity to 0.1 or to 10; dependences of the ratio on c are almost the same for the two values of τ . For comparison with the data of Beysens (2019), we plot (2.28) for $c = 0.25$ and 4 with red short bars in figure 3. It is clear for $\tau > 10^{-3}$ that the two bars at the same τ are closer to each other as τ is larger; (2.28) depends on c only when the suppression occurs. The range of c is considered as $1/2 \leq c \leq 2$ in § 2.2. For $c = 1/2$ (2), each of the results indicated by solid circles for $\tau \leq 1.61 \times 10^{-2}$ is shifted to the middle between the solid circle and the lower (upper) short bar. These slight shifts show that our results for any value of c in the interval of $1/2 \leq c \leq 2$ explain the experimental data well. It is also suggested that, if we take into account the dependence of c on θ in this interval, the calculation results should remain in good agreement with the experimental data.

Let us examine where the suppression occurs around a particle moving in the way supposed in figure 1. In the approximation mentioned below (2.12), we use $s^{(0)}$ instead of s in (2.5) to calculate $|\tilde{\eta}^{(1)}/\tilde{\eta}^{(0)}|$ for $c = 1$ and $U = \bar{U}$, and show the results in figure 5, where the suppression occurs in coloured regions. The maximum of (2.14) is taken at $(\rho, \theta) = (\sqrt{2}, 0)$ or $(\sqrt{2}, \pi)$. The value of $|\tilde{\eta}^{(1)}/\tilde{\eta}^{(0)}|$ equals κ at these points, and becomes smaller at a point more distant from these points, as shown in figure 5. The maximum of $\tau_{s^{(0)}}$ is $0.0129 \times c^{0.518}$ for $U = \bar{U}$, and is $0.0264 \times c^{0.518}$ for $U = 4\bar{U}$, which is approximately the effective cutoff in our numerical integration. The latter yields $\kappa \approx 0.13$ at $\tau = 10^{-3}$ and ≈ 0.21 at $\tau = 10^{-4}$ for $c = 1$ and $U = 4\bar{U}$. Thus, κ is adequately small as compared with unity in the range of τ examined in figure 3, which would make our formulation globally meaningful.

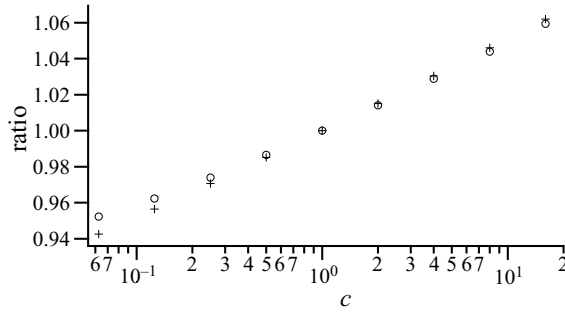


FIGURE 4. Ratios of D for some c values to D for $c = 1$ are calculated with the aid of (2.28) and plotted. The values of τ are 1.26×10^{-4} (+) and 1.008×10^{-3} (o).

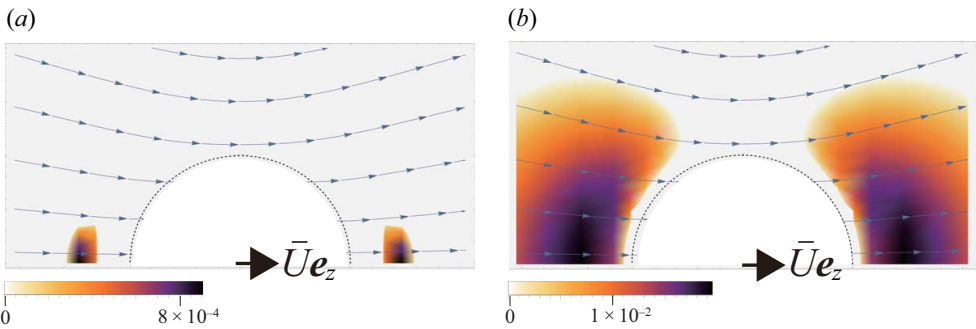


FIGURE 5. Colour gradation represents the largest of zero and $1 - \frac{\tau}{\tau_{s(0)}} v^{(d-z)}$ for $c = 1$ and $U = \bar{U}$ at each of $\tau = 1.26 \times 10^{-2}$ (a) and 8.064×10^{-3} (b). The particle is assumed to move translationally with the velocity $\bar{U}e_z$. The region shown in each figure is the same as in figure 1; the dotted curve represents the half of the cross-section of the particle surface. The curves outside the particle are the stream lines of $v^{(0)}$, which are represented by arrows in figure 1.

From the maximum of $\tau_{s(0)}$ for $U = \bar{U}$ mentioned above, κ is found to become non-zero when τ is smaller than 1.29×10^{-2} for $c = 1$ and $U = \bar{U}$. This value of τ approximately agrees with the onset temperature of the suppression estimated in Beysens (2019), where the shear rate, with its inhomogeneity and dependence on U being neglected, is evaluated to be a typical shear rate, \bar{U}/r_0 . The value of τ is slightly smaller than 1.29×10^{-2} in figure 5(a), where a very weak suppression occurs in narrow regions around $(\rho, \theta) = (\sqrt{2}, 0)$ and $(\sqrt{2}, \pi)$ for $c = 1$ and $U = \bar{U}$, as expected. However, at this temperature, the suppression cannot be read in figure 3. In figure 5(b) with smaller τ , $|\tilde{\eta}^{(1)}/\tilde{\eta}^{(0)}|$ becomes larger in wider regions, which means that the suppression occurs more strongly and extensively, although the suppression can be read only slightly from the solid circle at this temperature and cannot be read from the open circle closest to this temperature in figure 3. It is for $\tau < 3.2 \times 10^{-3}$ in figure 3 that the suppression can be read explicitly from the experimental data (o); the suppression for $c = 1$ and $U = \bar{U}$ should occur more strongly and extensively in this range of τ than in figure 5(b). Thus, we overestimate the onset temperature of the suppression in the data of the self-diffusion coefficient if we evaluate the shear rate to be \bar{U}/r_0 .

For $U = 4\bar{U}$, as mentioned above, the maximum of $\tau_{s^{(0)}}$ is $0.0264 \times c^{0.518}$. The maximum is smaller than unity in the range of c examined in [figure 4](#), as supposed in our formulation. This also shows that our results are free from the details of a formal rule for large particle speed in [appendix D](#). In the absence of the suppression, we have $\xi = \xi_0 \tau^{-\nu} = 28 \text{ nm}$ and 120 nm for $\tau = 10^{-3}$ and 10^{-4} , respectively. The correlation length should be reduced by the strong shear, which suppresses the order-parameter fluctuation with small wavenumber. The correlation length under the shear effect is dependent on the direction, and proportional to $\tau^{-0.5}$ at the largest in the stagnation-point flow (Onuki & Kawasaki 1980*c*). This exponent is the same as in the mean-field approximation. The curvature of the stream line in [figure 3](#) suggests that a typical length of the flow is several times larger than the particle diameter. Thus, a typical length of the flow is sufficiently large as compared with ξ in the range of τ examined in [figure 3](#), as supposed in our formulation.

It is assumed in (2.4) that the suppression is perfect if it occurs. In terms of the renormalization-group calculation, the singular part of the viscosity changes in the coarse-graining procedure, which makes sense until the resolution reaches ξ , and the way of the change is altered when the resolution exceeds a threshold determined by the shear rate. Equation (1.3) can be derived from the condition of whether the threshold comes before ξ or not, as mentioned in the latter half of [appendix A](#). In the procedure after the alteration, the singular part of the viscosity continues to be changed and becomes anisotropic. Thus, the assumption in (2.4) does not hold exactly. The ratio of the correction in the later stage, i.e. in the stage after the alteration, to the one in the earlier stage is evaluated by averaging the former correction over the directions in [appendix E](#). If $d = 3$ is substituted into these results valid up to the linear order with respect to $4 - d$, the evaluated ratio is smaller than 4 (7) per cent for a pure-extension flow (a simple shear flow). These small values would support the appropriateness of (2.4), which can explain the data for the three-dimensional mixture of Beysens (2019) in [figure 3](#).

In deriving (1.3), the lifetime of a correlated cluster and the range of the cluster size are evaluated. However, some deviations are possible in these evaluations, and may be required to compensate for the approximation in (2.4) mentioned above. For example, let us consider replacing ξ with 1.5ξ in (1.3). This replacement is equivalent with putting c equal to $1.5^z \approx 3.5$. A change of (1.3) to this extent cannot be denied from the data of Beysens (2019) in [figure 3](#), considering that the red short bars above the solid circles still lie in the middle of the distribution of the data.

We simply link the drag coefficient with the self-diffusion coefficient by means of the one-dimensional Langevin equation for the particle velocity. Similar nonlinear Langevin equations are used for different problems in Klimontovich (1994) and Lindner (2007). Validity of the Langevin equation with the Stratonovich interpretation in our problem, where the viscosity can be inhomogeneous and dependent on the particle speed, remains to be founded on the fluctuating hydrodynamics, unlike in the cases studied by Bedeaux & Mazur (1974) and Mazur & van der Zwan (1978). It still appears that the Langevin equation can describe the data of Beysens (2019) well in [figure 3](#), where a rather large distribution of the data for small τ in the direction of the vertical axis may come from the properties of the viscosity in our problem.

4. Summary and concluding remarks

Correlated clusters of the order-parameter fluctuation are generated in a near-critical binary fluid mixture lying in the homogeneous phase near the demixing critical point. The upper size of clusters, the correlation length, becomes larger as the critical point

is approached. Then, as is well known, the convection of large and long-lived clusters enhances the transport coefficients in the coarse-grained dynamics (Kawasaki 1970). It is also well known that a sufficiently strong shear, if imposed, can deform long-lived clusters to suppress the critical enhancement (Onuki & Kawasaki 1979). In a recent experiment (Beysens 2019), shear around a Brownian particle in a near-critical mixture on the critical isochore was suggested to cause this suppression to influence the motion. Deviation of the self-diffusion coefficient from the Stokes–Sutherland–Einstein formula was observed in the temperature range where the suppression is judged to occur from a typical shear rate around a particle moving with a typical speed.

How the deviation depends on the temperature is calculated in the present study. We first calculate the drag coefficient of a particle moving translationally in a mixture which is quiescent far from the particle. The suppression is simply assumed to occur perfectly when the cluster with the size of the correlation length becomes so long-lived as to be deformed by the shear. The shear rate is inhomogeneous and depends on the particle speed. Hence, the suppression makes the viscosity inhomogeneous and dependent on the particle speed. The calculation supposes a low Reynolds-number and a sufficiently weak influence of the shear on the viscosity, which are realized in the experiment. We next employ the drag coefficient thus calculated, dependent on the particle speed, as the frictional coefficient in a one-dimensional Langevin equation of the Stratonovich type to calculate the self-diffusion coefficient. The calculation results agree well with the experimental data, which is rather robust to changes in the threshold for the occurrence of the suppression.

Acknowledgements

The author thanks S. Yabunaka for helpful discussions.

Declaration of interests

The author reports no conflict of interest.

Appendix A. Previous results of the renormalization-group calculations

For an equilibrium binary fluid mixture in the homogeneous phase on the critical isochore near the critical point, as the renormalization steps are iterated, the Onsager coefficient for the interdiffusion approaches a constant, denoted by λ^* . Rewinding the rescaling procedure to decrease the cutoff wavenumber k at each iteration, we obtain the coefficient coarse grained up to k . Writing λ for it, we have

$$\lambda = \lambda^* \left(\frac{k_o}{k} \right)^{4-\eta-z} \quad \text{if } k\xi \gtrsim 1, \quad (\text{A } 1)$$

that is, if $k\xi$ is larger than or comparable to unity. Here, $k_o (\gg k)$ is the cutoff wavenumber before coarse graining and thus $1/k_o$ has a microscopic length. If $k\xi$ is much smaller than unity, $1/k$ in the parentheses of (A 1) should be replaced by ξ ; rewinding the rescaling procedure makes sense up to the length scale of ξ . Likewise, the singular part of $\tilde{\eta}$ is given by $\tilde{\eta}^*(k_o/k)^{z-d}$ for $\xi^{-1} \lesssim k \ll k_o$ and

$$\tilde{\eta}^*(k_o\xi)^{z-d} \quad \text{if } k\xi \ll 1, \quad (\text{A } 2)$$

where $\tilde{\eta}^*$ denotes a constant for $\tilde{\eta}$ corresponding with λ^* (Onuki & Kawasaki 1979). These exponents can be also derived from the dynamic scaling assumption (Folk & Moser 2006).

We define the order parameter so that the coefficient of the square-gradient term in the dimensionless effective Hamiltonian is a half, as in Siggia *et al.* (1976), Onuki & Kawasaki (1979) and Onuki (2002). In the Fourier transform mentioned above (1.1), we put the two times equal to each other and write χ_k for the result, which is the static correlation function or static susceptibility. We have $\chi_k \approx \xi^2(k/k_o)^n$ for $k\xi \ll 1$. As $k \rightarrow 0$ and $\xi \rightarrow \infty$ with $k\xi$ being an arbitrary positive number, the renormalization-group calculation gives (Siggia *et al.* 1976)

$$\Gamma_k = \frac{Rk_B T_c}{\tilde{\eta}\xi^{d-2}} k^2 \bar{\Omega}(k\xi), \tag{A 3}$$

where the Kawasaki amplitude R is a universal constant approximately equal to $1/(6\pi)$. The dimensionless scaling function, $\bar{\Omega}$, tends to unity as its variable approaches zero. Considering that $\lambda\tilde{\eta}\xi^{d-2}$ divided by χ_k equals $Rk_B T_c$ for $k\xi \ll 1$, we have

$$\frac{\Gamma_k}{k^2} \rightarrow \lambda^* k_o^{4-z} \xi^{2-z} \quad \text{as } k \rightarrow 0 \tag{A 4}$$

with $k\xi$ being fixed to be small (Siggia *et al.* 1976).

According to the renormalization-group calculation up to the order of $\epsilon \equiv 4 - d$ in the presence of a simple shear flow (Onuki & Kawasaki 1979), (A 1) is found to break down for $k \lesssim k_s$, where k_s is defined so that

$$\lambda^* k_o^{4-z} k_s^z = s \tag{A 5}$$

holds. The shear is strong enough to suppress the critical enhancement if $k_s \xi \gtrsim 1$ holds; k_s then comes before $1/\xi$ in the coarse-graining process of decreasing k (figure 6). Otherwise, λ for $k\xi \ll 1$ remains given by (A 1) with $1/k$ being replaced by ξ . With the aid of (A 3)–(A 5), we find that this condition of strong shear approximately agrees with (1.3). From (2.3) and (A 5), we have $k_s^{-1} = \xi_0 \tau_s^{-\nu}$ and

$$s^* \equiv \lambda^* k_o^{4-z} \xi_0^{-z}. \tag{A 6}$$

Ambiguity on the condition of strong shear is discussed in § 3.

The above-mentioned breakdown of (A 1) occurs when the static susceptibility deviates from the Ornstein–Zernike form in the mean-field approximation for an equilibrium fluid mixture. Then, using the wavenumber vector \mathbf{k} , we should write $\chi_{\mathbf{k}}$, not χ_k , for the susceptibility because of its anisotropy. The method of characteristics is used to calculate $\chi_{\mathbf{k}}$ for a simple shear flow in § 3 of Onuki & Kawasaki (1979), and for other kinds of linear shear flow in § 4 of Onuki & Kawasaki (1980a) and § 3 of Onuki & Kawasaki (1980c). In this method, a wavenumber vector dependent on a parameter, with the dimension of the time, is introduced, and the ‘time’ derivative of the vector equals the product of the matrix of the velocity gradient and the vector. Thus, s in (1.3) can be determined in the way described in § 1.

The renormalization correction of λ in the later stage with $k < k_s$ in a simple shear flow becomes dependent not only on k but also on \mathbf{k} , and is much smaller than the one in the earlier stage with $k > k_s$ even when ϵ is put equal to unity, as shown by (4.62) and (4.85) of Onuki & Kawasaki (1979). We draw figure 6 from figure 2 of Onuki & Kawasaki (1979), where it is stated that the singular part of the viscosity behaves in the same fashion, although the viscosity for $k < k_s$ is not only dependent on \mathbf{k} but also expressed in terms of

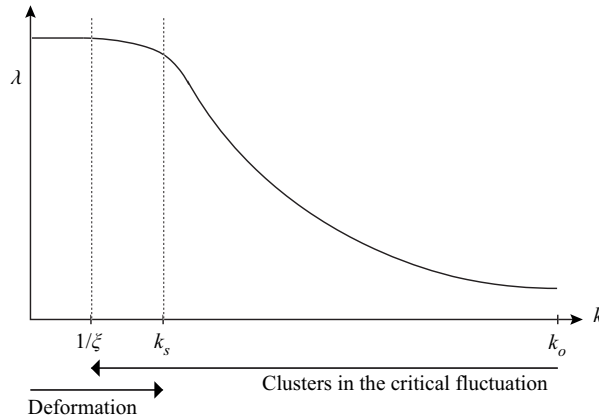


FIGURE 6. A schematic graph showing how λ changes as the mixture is coarse grained, which is made from figure 2 of Onuki & Kawasaki (1979). We define k so that the cutoff wavenumber viewed on the original lattice equals k at the iteration number, l , in the renormalization-group calculation. We have $k/k_o = \tilde{b}^{-l}$, where \tilde{b} is the length rescaling factor. The curve follows (A 1) for $k_o \gg k \gg k_s$, but deviates from (A 1) for $k_s \gtrsim k$.

an anisotropic tensor (Onuki & Kawasaki 1980b). Within a simplified picture of figure 6, assuming (2.4) amounts to drawing the curve of the singular part of $\tilde{\eta}$ as if the curve for $k \geq k_s$ were perfectly free from the shear effect and linked to a horizontal line in $k < k_s$.

Appendix B. Local shear rate

We here examine how $\nabla v^{(0)}$ changes around a particle, which is briefly mentioned above (2.14). From (2.8a–c), we can calculate the components of $\nabla v^{(0)}$ with respect to the three-dimensional Cartesian coordinates (x, y, z) at a point on the xz plane ($\phi = 0$). There, the (x, y) , (y, x) , (y, z) and (z, y) components vanish. The components can be expressed in terms of a 3×3 matrix. We rewrite this matrix as the sum of two matrices; one is the diagonal matrix with the diagonal elements being

$$(\nabla_x v_x^{(0)} + \nabla_z v_z^{(0)})/2, \quad \nabla_y v_y^{(0)} \quad \text{and} \quad (\nabla_x v_x^{(0)} - \nabla_z v_z^{(0)})/2 \tag{B 1a–c}$$

from the top. We rotate the (x, z) coordinates to have (x', z') coordinates so that the diagonal elements of the other matrix of the two vanish at the point; the diagonal matrix mentioned above is not changed by this rotation. The components of the velocity gradient with respect to the coordinates (x', y, z') are given by

$$\frac{U}{r_0} \left[\begin{pmatrix} -C/2 & 0 & 0 \\ 0 & C & 0 \\ 0 & 0 & -C/2 \end{pmatrix} + \begin{pmatrix} 0 & 0 & B - A \\ 0 & 0 & 0 \\ B + A & 0 & 0 \end{pmatrix} \right], \tag{B 2}$$

where we use $A \equiv 3 \sin \theta / (4\rho^2)$. We define C as $\nabla_y v_y^{(0)} = 3(\rho^2 - 1) \cos \theta / (4\rho^4)$, and define B as $3 / (8\rho^4)$ multiplied by the square root of

$$[-2 + 2(5 - 3\rho^2) \cos^2 \theta]^2 \sin^2 \theta + [3(\rho^2 - 1) + 2(5 - 3\rho^2) \sin^2 \theta]^2 \cos^2 \theta. \tag{B 3}$$

Thus, A and B are non-negative. The first term in the square brackets of (B 2) represents a pure-extension flow.

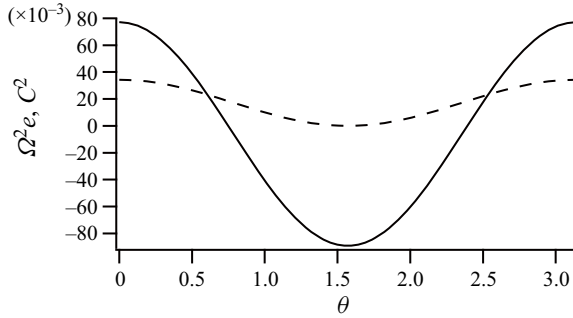


FIGURE 7. We plot Ω_e^2 (solid curve) and C^2 (dashed curve) at $\rho = 1.5$ against θ .

We define Ω_e as $\sqrt{B^2 - A^2}$, and have

$$\Omega_e^2 = \frac{9(\rho^2 - 1)}{128\rho^8} [5\rho^2 - 13 + (13\rho^2 - 5) \cos 2\theta], \tag{B 4}$$

which vanishes at $\rho = 1$. As mentioned in the fourth paragraph of § 1, the exponential of the product of (B 2) and the time t works as the time evolution operator for a convected line segment. The long-wavelength fluctuations of the order parameter are suppressed in the stretching direction. The exponential equals

$$\begin{pmatrix} e^{-\check{C}t/2} \cosh \Omega_e \check{t} & 0 & (B - A) \Omega_e^{-1} e^{-\check{C}t/2} \sinh \Omega_e \check{t} \\ 0 & e^{\check{C}t} & 0 \\ (B + A) \Omega_e^{-1} e^{-\check{C}t/2} \sinh \Omega_e \check{t} & 0 & e^{-\check{C}t/2} \cosh \Omega_e \check{t} \end{pmatrix} \tag{B 5}$$

where we use $\check{t} \equiv tU/r_0$ and note that the matrices in the square brackets of (B 2) commute. In figure 7 with $\rho = 1.5$, we have $A > B$, i.e. purely imaginary Ω_e , for $0.74 < \theta < 2.4$ approximately, and $C^2 > \Omega_e^2$ for $0.6 < \theta < 2.5$ approximately. Although data are not shown, as ρ increases above unity, the θ region with $A > B$ and the one with $C^2 > \Omega_e^2$ are narrower. We find that $A > B$ holds at $\theta = \pi/2$ for any ρ larger than unity and that $\Omega_e = 1.5|C|$ holds at $\theta = 0$ and π . As θ changes from 0 or π to $\pi/2$, Ω_e^2 decreases more rapidly than C^2 , as shown in figure 7. The two-dimensional flow with $C = 0$ is considered in Onuki & Kawasaki (1980c), where a rotational flow with $A > B$ is shown to be weak in suppressing the critical enhancement. For simplicity, we thus neglect the periodic deformation of a cluster in determining the local shear rate.

We suppose $U > 0$ in this paragraph. In the components of (B 5), when Ω_e is real, the largest stretching rate is CU/r_0 if $C > 0$ and is $(2\Omega_e - C)U/(2r_0)$ if $C < 0$. When Ω_e is imaginary, the largest stretching rate is CU/r_0 if $C > 0$ and is $-CU/(2r_0)$ if $C < 0$. These results agree with (2.14), considering that (2.14) with $c = 1$ equals $|CU|/r_0$. We find for $U > 0$ that c is unity for $0 \leq \theta \leq \pi/2$, is 1/2 for $\pi/2 < \theta \leq \pi$ and $\Omega_e^2 < 0$, and increases up to 2 as θ increases in the region of $\pi/2 < \theta \leq \pi$ and $\Omega_e^2 \geq 0$.

Appendix C. Some details in calculating the drag force

We introduce

$$\Gamma_J^{(com)}(\rho, \sigma) \equiv \frac{1}{4\rho^{J+2}\sigma^{J+2}} \left[\frac{1}{2J+3} - \frac{\sigma^2}{2J+1} \right] + \frac{1}{4\rho^J\sigma^{J+2}} \left[\frac{\sigma^2}{2J-1} - \frac{1}{2J+1} \right], \tag{C 1}$$

and the kernel appearing in (2.22) is given by

$$\Gamma_J(\rho, \sigma) \equiv \Gamma_J^{(com)}(\rho, \sigma) + \frac{\sigma^{J-1}}{2\rho^{J+2}(2J+1)} \left[\frac{\sigma^2}{2J+3} - \frac{\rho^2}{2J-1} \right] \quad \text{for } \rho > \sigma, \quad (C2)$$

together with $\Gamma_J(\rho, \sigma) = \Gamma_J(\sigma, \rho)$ for $\rho < \sigma$. The kernel above for $J = 1$ is equal to $1/30$ multiplied by Γ_R of Okamoto *et al.* (2013). Similar calculations are there in Fujitani (2018) and Yabunaka & Fujitani (2020).

As mentioned above (2.23), we can delete Π_J and T_J from the last two terms of (2.13). A similar procedure can be found in deriving (4.19) of Okamoto *et al.* (2013). By using

$$-\frac{1}{2} \int_0^\pi d\theta \sin^2 \theta \frac{\partial}{\partial \theta} Y_{J0}(\cos \theta) = \int_0^\pi d\theta \sin \theta \cos \theta Y_{J0}(\cos \theta) = \frac{\delta_{J1}}{\sqrt{\pi(2J+1)}}, \quad (C3)$$

where δ_{ij} implies the Kronecker delta, we find the surface integral of the last two term of (2.13) to be given by

$$-\frac{2\sqrt{3\pi}}{3} \tilde{\eta}^{(0)} r_0 \left(\frac{1}{2} \partial_\rho^3 + 2\partial_\rho^2 \right) R_1 - \frac{\sqrt{6\pi}}{3} r_0^3 H_1(1). \quad (C4)$$

Differentiating (2.5) with respect to ρ or θ yields a term having the derivative of the step function, i.e. the delta function. Noting that this term vanishes because of its prefactor, we find that the negative of the right-hand side of (2.12) can be rewritten as

$$\frac{3U\tilde{\eta}^{(0)}}{r_0^2} \mathbf{h}^\Theta(\check{\tau}_{s^{(0)}} - 1). \quad (C5)$$

Here, the vector \mathbf{h} dependent on (ρ, θ) can be calculated by using (2.8a–c). Because (2.17) is equal to (C5), we use the orthogonality of the vector spherical harmonics to calculate F_1 and H_1 . For example, $H_1(\rho)$ is the integral of the inner product of vectors of (C5) and \mathbf{B}_{10} over the surface of the unit sphere. We thus find that $H_1(\rho)$ vanishes at $\rho = 1$, where (2.14), and thus $\check{\tau}_{s^{(0)}}$ vanish.

Substituting (2.8a–c) into the right-hand side of (2.12) and defining ζ as $(d/z) - 1$, we find that the components of \mathbf{h} are given by

$$\left. \begin{aligned} h_r(\rho, \theta) &= \left\{ \frac{1 - \check{\tau}_s^{\nu(d-z)}}{\rho^3} + \zeta \check{\tau}^{\nu(d-z)} \left[\frac{1 - \rho^2}{\rho^4 s} \frac{\partial s}{\partial \rho} + \frac{1}{2\rho^5 s} \frac{\partial s}{\partial \theta} \tan \theta \right] \right\} \cos \theta, \\ h_\theta(\rho, \theta) &= \left\{ \frac{1 - \check{\tau}_s^{\nu(d-z)}}{2\rho^3} + \zeta \check{\tau}^{\nu(d-z)} \left[\frac{1}{2\rho^4 s} \frac{\partial s}{\partial \rho} + \frac{\rho^2 - 1}{2\rho^5 s} \frac{\partial s}{\partial \theta} \cot \theta \right] \right\} \sin \theta, \end{aligned} \right\} \quad (C6)$$

and $h_\phi = 0$, where we write s for $s^{(0)}$ for conciseness. We have $h_r(\rho, \theta) = -h_r(\rho, \pi - \theta)$ and $h_\theta(\rho, \theta) = h_\theta(\rho, \pi - \theta)$. From (2.20) for $J = 1$, we obtain

$$\check{X}(\rho) = -\frac{\rho^2}{2} \int_0^{\pi/2} d\theta [2 \sin \theta \cos \theta h_r(\rho, \theta) + \sin^2 \theta \partial_\rho h_\theta(\rho, \theta)] \Theta(\check{\tau}_{s^{(0)}} - 1), \quad (C7)$$

where ∂_ρ operates on all the following terms including the step function.

Substituting (C 7) into (2.24), we employ integration by parts with respect to ρ , and the resultant integrand contains the step function, not its derivative. Writing \check{U}_c for $c|U|/U^*$, we have

$$\check{\tau}_{s(0)}(\rho, \theta) = \frac{1}{\tau} \left[\frac{3(\rho^2 - 1)}{4\rho^4} \check{U}_c \cos \theta \right]^{1/(\nu z)} \tag{C 8}$$

in (C 7). Thus, the step function in (C 7) can be non-zero if

$$4\rho^4 - 3\tau^{-\nu z} \check{U}_c (\rho^2 - 1) \cos \theta < 0, \tag{C 9}$$

whose left-hand side is quadratic with respect to ρ^2 . Putting the left-hand side above equal to zero gives $\rho = \rho_{\pm}$ and $\rho = -\rho_{\pm}$, where ρ_{\pm} is defined as

$$\rho_{\pm}(\theta) \equiv \left(\frac{3\check{U}_c}{8\tau^{\nu z}} \cos \theta \pm \frac{\sqrt{\Delta(\theta)}}{2} \right)^{1/2}. \tag{C 10}$$

Here, Δ is the discriminant, given by

$$\Delta(\theta) \equiv \frac{3\check{U}_c}{\tau^{\nu z}} \left(\frac{3\check{U}_c}{16\tau^{\nu z}} \cos \theta - 1 \right) \cos \theta. \tag{C 11}$$

Equation (2.24) does not vanish if Δ is positive and if $\rho_- < \rho < \rho_+$, where we have $1 < \rho_- < \rho_+$ for $\Delta > 0$.

We introduce

$$G_{m,n}(\theta) \equiv \Theta(\Delta(\theta)) \int_{\rho_-(\theta)}^{\rho_+(\theta)} d\rho \left(\frac{\rho^2 - 1}{\rho^4} \right)^{\zeta - m} \frac{1}{\rho^n}, \tag{C 12}$$

which is expressed in terms of Gauss' hypergeometric function according to Mathematica (Wolfram Research). The integral of (2.24) is found to be the sum of the integrals of the following three integrands over $0 < \theta < \pi/2$. The integrands are

$$\Theta(\Delta(\theta)) \int_{\rho_-(\theta)}^{\rho_+(\theta)} d\rho \left(\frac{3\rho^2 + 1}{4\rho^4} \sin^3 \theta + \frac{1 - 3\rho^2}{\rho^4} \sin \theta \cos^2 \theta \right), \tag{C 13}$$

where the integration with respect to ρ is elementary,

$$- \left(\frac{3\check{U}_c}{4\tau^{\nu z}} \right)^{\zeta} \frac{1}{4} [3G_{0,2} + G_{0,4} + \zeta (3G_{1,4} - 5G_{1,6} - G_{1,8} - 5G_{1,10})] \cos^{\zeta} \theta \sin^3 \theta \tag{C 14}$$

and

$$\left(\frac{3\check{U}_c}{4\tau^{\nu z}} \right)^{\zeta} [3G_{0,2} - G_{0,4} - \zeta (6G_{0,2} - 14G_{0,4} + 4G_{0,6})] \cos^{\zeta+2} \theta \sin \theta, \tag{C 15}$$

where the variable θ of $G_{m,n}$ is dropped for conciseness.

Appendix D. Self-diffusion coefficient

The Fokker–Planck equation corresponding to (2.26) is

$$\frac{\partial}{\partial t}P(U, t; U_0) = \frac{1}{m} \frac{\partial}{\partial U} (\gamma UP) + \frac{1}{2m^2} \frac{\partial}{\partial U} b \frac{\partial}{\partial U} bP, \tag{D 1}$$

where $P(U, t; U_0)$ represents the probability density of U at a time t on condition that $U = U_0$ at $t = 0$. The variables of the functions are dropped on the right-hand side above for conciseness. The stationary solution, denoted by $P_{eq}(U)$, is proportional to (Risken 2002)

$$\frac{m^2}{b^2} \exp \left[\int dU \left(\frac{1}{2b^2} \frac{db^2}{dU} - \frac{2m\gamma U}{b^2} \right) \right], \tag{D 2}$$

which should be proportional to the Boltzmann distribution (Zwanzig & Bixon 1975),

$$\sqrt{\frac{m}{2\pi k_B T}} e^{-mU^2/(2k_B T)}. \tag{D 3}$$

Considering that b^2 equals $2\gamma k_B T$ if $\gamma(U)$ is independent of U , we find

$$b(U)^2 = 4me^{mU^2/(k_B T)} \int_U^\infty dU_1 \gamma(U_1) U_1 e^{-mU_1^2/(k_B T)}. \tag{D 4}$$

We can rewrite the right-hand side above by changing the integration interval to the one from U to $-\infty$ because the integral from $-\infty$ to ∞ vanishes. Then, using integration by parts, we find that $|b(U)^2 - 2k_B T \gamma(U)|$ equals

$$2k_B T e^{mU^2/(k_B T)} \left| \int_{-U}^\infty dU_1 \gamma'(U_1) e^{-mU_1^2/(k_B T)} \right|, \tag{D 5}$$

where the prime indicates the derivative. We can assume that $\check{\gamma}(u)$ decreases to a positive constant as $|u|$ increases to ∞ for the reason mentioned in the next paragraph. Thus, for $U < 0$, (D 5) becomes larger if we replace $\gamma'(U_1)$ with a suitable positive constant. Using an asymptotic form of a complementary error function, we find that (D 5) vanishes, and thus $b(U)^2$ remains finite, in the limit of $U \rightarrow -\infty$. This result is used later.

We can make a convenient formal rule for the particle speed larger than assumed in the text, because we later find its influence on (2.28) negligible. In other words, making such a rule is a substitute for introducing an upper cutoff of the particle speed to the model in the text. For definiteness, we here specify a formal rule. In (2.1), we should replace τ with unity for $\tau > 1$. Accordingly, (2.4) is supplemented with the rule $\tilde{\eta} = \tilde{\eta}_B(T)$ for $\tau > 1$ if $\tau_s < 1$ and for any τ otherwise. As the particle speed is larger, because the region with $\tau_s > 1$ approaches the whole mixture region, $\gamma(U)$ approaches Stokes' law of $6\pi\tilde{\eta}_B(T)r_0$ from the larger side. This means that $\check{\gamma}(\infty)$ is not smaller than $\tau^{\nu(\tau-d)}$, which is 0.75 and 0.68 for $\tau = 10^{-3}$ and 10^{-4} , respectively. Thus, the assumption mentioned in the preceding paragraph holds in the range of τ of figure 3.

Introducing a Laplace transform, defined as

$$\hat{Q}(U, \sigma; U_0) \equiv \int_0^\infty dt [P(U, t; U_0) - P_{eq}(U)] e^{-\sigma t}, \tag{D 6}$$

we use $\langle U_0 \rangle = 0$ to rewrite (2.27) as

$$D = \int_{-\infty}^\infty dU \int_{-\infty}^\infty dU_0 UU_0 \hat{Q}(U, 0; U_0) P_{eq}(U_0). \tag{D 7}$$

From the Laplace transform of (D 1), we use (D 2) and (D 3) to obtain

$$-\delta(U - U_0) + P_{eq}(U) = \frac{1}{2m^2} \frac{\partial}{\partial U} b^2(U) P_{eq}(U) \frac{\partial}{\partial U} \frac{\hat{Q}(U, 0; U_0)}{P_{eq}(U)}, \tag{D 8}$$

where δ represents the delta function. With \mathcal{O} indicating the Landau symbol, we have $\hat{Q}(U, \sigma; U_0) < \mathcal{O}(|U|^{-1})$ as $|U| \rightarrow \infty$ because the normalization conditions of P and P_{eq} give

$$\int_{-\infty}^\infty dU \hat{Q}(U, \sigma; U_0) = 0. \tag{D 9}$$

As mentioned above, $b(U)^2$ remains finite in the limit of $U = -\infty$. Integrating (D 8) with respect to U from $-\infty$ gives

$$\frac{2m^2}{b^2(U)P_{eq}(U)} \left[-\Theta(U - U_0) + \int_{-\infty}^U dU_1 P_{eq}(U_1) \right] = \frac{\partial}{\partial U} \frac{\hat{Q}(U, 0; U_0)}{P_{eq}(U)}. \tag{D 10}$$

Integrating (D 10) with respect to U from a value smaller than U_0 , substituting the result into (D 7) and using $\langle U_0 \rangle = 0$, we arrive at

$$D = -2m^2 \int_{-\infty}^\infty dU \int_{-\infty}^\infty dU_0 UU_0 P_{eq}(U) P_{eq}(U_0) \int_{U_0}^U dU_1 \frac{1}{b(U_1)^2 P_{eq}(U_1)}. \tag{D 11}$$

Interchanging the order of the integrals above, we use $\check{\gamma}(u) = \check{\gamma}(-u)$ to obtain (2.28).

Some details on numerical calculations of (2.28) are mentioned below. We define L as

$$L(u_a, u_b) = \int_{u_a}^{u_b} du_1 \check{\gamma}(u_1) u_1 e^{-Mu_1^2}. \tag{D 12}$$

We can choose $u_c (> 0)$ so that $|\check{\gamma}'(u)|$ is smaller than $|\check{\gamma}'(u_c)|$ for $u > u_c$. The integral in the square brackets of (2.28) is given by $L(u, \infty)$. Using integration by parts, we obtain

$$L(u_c, \infty) = \frac{\check{\gamma}(u_c)}{2M} e^{-Mu_c^2} \left[1 + \frac{e^{Mu_c^2}}{\check{\gamma}(u_c)} \int_{u_c}^\infty du_1 \check{\gamma}'(u_1) e^{-Mu_1^2} \right]. \tag{D 13}$$

The absolute value of the second term in the square brackets above is smaller than

$$\frac{|\check{\gamma}'(u_c)| e^{Mu_c^2}}{\check{\gamma}(u_c) \sqrt{M}} \int_{u_c \sqrt{M}}^\infty dx e^{-x^2} \approx \frac{|\check{\gamma}'(u_c)|}{2Mu_c \check{\gamma}(u_c)}, \tag{D 14}$$

where the approximation is good for $u_c \sqrt{M} \gtrsim 1$. In our numerical calculations, we choose u_c so that $u_c \sqrt{M} \approx 4$, and find that the right-hand side above is smaller than 10^{-3} , which enables us to neglect the second term in the square brackets of (D 13).

The integral with respect to u in (2.28) is rewritten as

$$\int_0^{u_c} du \frac{e^{-3Mu^2/2}}{L(u, \infty)} + \int_{u_c}^{\infty} du \frac{e^{-3Mu^2/2}}{L(u, \infty)}, \tag{D 15}$$

where u_c is chosen as indicated above. In the first term above, we can use

$$L(u, \infty) \approx L(u, u_c) + \frac{\tilde{\gamma}(u_c)}{2M} e^{-Mu_c^2}. \tag{D 16}$$

In the second term of (D 15), because of $u > u_c$, $L(u, \infty)$ can be approximated to be the second term on the right-hand side of (D 16) with u_c being replaced by u for the same reason as described in the preceding paragraph. Thus, the second term of (D 15) is approximately equal to

$$\frac{2M}{\check{\gamma}(u_c)} \int_{u_c}^{\infty} du e^{-Mu^2/2}. \tag{D 17}$$

Here, we use $\check{\gamma}(u_c) \approx \check{\gamma}(\infty)$. In our numerical calculation, with u_c being chosen as indicated above, the ratio of (D 17) to the first term of (D 15) is much smaller than 10^{-3} , and thus the first term is regarded as equal to the integral with respect to u in (2.28). Hence, we can calculate (2.28) by using $\check{\gamma}(u)$ with $u \leq u_c$, or in other words, by using $\gamma(U)$ with U smaller than $4\bar{U}$ approximately. Thanks to this effective cutoff speed, our calculation results are free from the details of the rule for a large particle speed, as checked quantitatively in § 3.

Appendix E. Renormalization correction under the shear effect

A simple shear flow in four dimensions is used in the calculation mentioned above (A 5). The components of its velocity gradient with respect to the Cartesian coordinates vanish except for $\nabla_2 v_1$, which is a positive constant. As mentioned at the end of appendix A, the singular part of the viscosity changes as k decreases from k_o . The ratio of the change in the later stage with $k < k_s$, to the change in the earlier stage with $k > k_s$, is given by the second term in the square brackets of (4.64) of Onuki & Kawasaki (1979). To evaluate this ratio, we take average of the term over the orthogonal components and average over the directions of the wavenumber vector. The former average is obtained by dividing (4.65) of Onuki & Kawasaki (1979) by three – the dimension of the divergence-free space. In this equation, the dot immediately after the fraction should be deleted to validate the equality, and the right-hand side, as it is, represents the trace of the left-hand side. The latter average is obtained by replacing \hat{k} in (4.65) of Onuki & Kawasaki (1979) by one of the four orthogonal unit vectors, summing the results over the four vectors, and dividing the sum by the spatial dimension, four. The result derived from these averages is denoted by δ_s . As in deriving the right-hand side of (3.6) of Onuki & Kawasaki (1979), we use the method of characteristics to find δ_s to be given by $4\epsilon/(19\pi^2)$ multiplied by the integral of

$$\frac{2}{q_1} (q_1^2 q_3^2 + q_1^2 q_4^2 + q_3^2 q_4^2) I(q) \tag{E 1}$$

with respect to the four-dimensional vector q over half the unit sphere with $q_1 > 0$, where $I(q)$ is defined as the integral of the following integrand over p running from q_2 to ∞ .

The integrand is given by

$$\exp \left[\frac{2}{3q_1} \left\{ \frac{3}{5}(q_2^5 - p^5) + (q_1^2 + q_3^2 + q_4^2)[2(q_2^3 - p^3) + 3(q_2 - p)] \right\} \right] \tag{E 2}$$

divided by $(0.97|q_1|^{2/5} + q_1^2 + p^2 + q_3^2 + q_4^2)^2$. If we replace this denominator by q^4 , where q denotes $|q|$, (E 1) becomes larger. Putting $q_3 = q_4 = 0$ and changing the variable p to $Z \equiv 2(p - q_2)/q_1$ in (E 2), we obtain a new exponential function. Its integral over $0 < Z < \infty$ is denoted by $I_1(q_1, q_2)$, and we have

$$\delta_s < \frac{4\epsilon}{19\pi^2} \int d\mathbf{q} \frac{q_1^2 q_3^2 + q_1^2 q_4^2 + q_3^2 q_4^2}{q^4} I_1(q_1, q_2), \tag{E 3}$$

where the integral is taken over half the unit sphere mentioned above. In the square brackets of (E 2) after the above-mentioned conversion, the leading term for large Z is given by $-q_1^4 Z^5/80$. Thus, as q_1 approaches zero from the positive side, the leading term of $I_1(q_1, q_2)$ is proportional to $q_1^{-4/5}$, which justifies that we neglected the contribution from the integrand with $q_1 = 0$ to the integral of (E 1). This integral shows $\delta_s > 0$.

Introducing the polar coordinates of q , we can numerically perform the integral of (E 3) over the angular components. We write $J(q, Z)$ for the result, and have

$$\delta_s < \frac{4\epsilon}{19\pi^2} \int_0^1 dq \int_0^\infty dZ J(q, Z). \tag{E 4}$$

If we retain only the leading term in (E 2), $J(q, Z)$ in (E 4) is replaced by

$$J_1(q, Z) \equiv \frac{2\pi q^3}{15} \int_0^{\pi/2} d\theta_1 e^{-q_1^4 Z^5/80} (20 - 18 \sin^2 \theta_1) \sin^4 \theta_1, \tag{E 5}$$

where θ_1 is defined so that $q_1 = q \cos \theta_1$ holds. The integral in (E 5) can be expressed in terms of generalized hypergeometric functions, and the integral of $J_1(q, Z)$ over $0 < Z < \infty$ turns out to be proportional to $q^{11/5}$, according to Mathematica (Wolfram Research). Numerically, $J(q, Z)$ is shown in figure 8 to be smaller than $J_1(q, Z)$. The double integral in (E 4) with J replaced by J_1 equals 3.44, which leads to $0 < \delta_s < 7.33 \times 10^{-2}\epsilon$.

In a pure-extension flow in four dimensions, the off-diagonal elements of the velocity gradient vanish and $\nabla_1 v_1 = -3\nabla_2 v_2 = -3\nabla_3 v_3 = -3\nabla_4 v_4$ is a positive constant. For this flow, we below evaluate the ratio of the changes in the later and earlier stages by taking averages in the same way as mentioned above, and write δ_e for the result corresponding with δ_s . The ratio should be given by (4.65) of Onuki & Kawasaki (1979) with the denominator being replaced by $q^4 - (q_1/2)\partial_{q_1} + (q_2/6)\partial_{q_2} + (q_3/6)\partial_{q_3} + (q_4/6)\partial_{q_4}$ and with the expression of the normalized susceptibility, denoted by $\chi^*(q)$, being replaced by the one for the flow considered here. With the aid of (3.4) of Onuki & Kawasaki (1980a), $\chi^*(q)$ is approximated to be $\sqrt{\pi}/2$ for $q_1 \neq 0$ in the pure-extension flow, as is consistent with (3.23b) of Onuki & Kawasaki (1980c). Thus, we find δ_e to be given by $4\epsilon/(19\pi^2)$ multiplied by the double integral of the following integrand over the unit sphere of the four-dimensional vector q and over $w = 0$ to ∞ . With q_\perp^2 denoting $q^2 - q_1^2 \equiv q^2 \sin^2 \theta_1$,

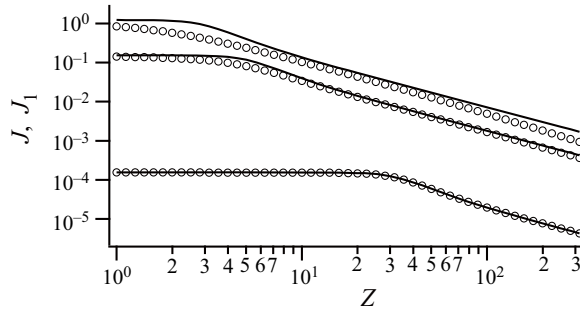


FIGURE 8. From the top, three solid curves, respectively, represent $J_1(1.0, Z)$, $J_1(0.5, Z)$ and $J_1(0.05, Z)$, while three series of circles, respectively, represent $J(1.0, Z)$, $J(0.5, Z)$ and $J(0.05, Z)$. We calculate $J(q, Z)$ by means of numerical integration in Mathematica (Wolfram Research) with Method \rightarrow {'GlobalAdaptive', 'MaxErrorIncreases' \rightarrow 10 000, Method \rightarrow 'GaussKronrodRule'}, MaxRecursion \rightarrow 20.

the integrand is the product of

$$\exp \left[\frac{q_1^4}{2} (1 - e^{4w}) + 3q_1^2 q_\perp^2 (1 - e^{4w/3}) + \frac{3q_\perp^4}{2} (e^{-4w/3} - 1) \right], \quad (\text{E } 6)$$

which is larger if we delete the last two terms in the square brackets, and

$$\frac{\pi}{4} \left[e^{2w/3} q_1^2 q_\perp^2 + e^{-2w/3} (q_2^2 q_3^2 + q_2^2 q_4^2 + q_3^2 q_4^2) \right], \quad (\text{E } 7)$$

which is larger if we replace $e^{-2w/3}$ with $e^{2w/3}$ in the second term in the square brackets. This expression shows $\delta_e > 0$. Using a new variable $\zeta_1 \equiv e^{2w/3}$, and performing the integration with respect to the angular components of \mathbf{q} other than θ_1 , we have

$$\delta_e < \frac{4\epsilon}{19\pi^2} \times \frac{3\pi^2}{10} \int_0^1 dq q^7 \int_0^\pi d\theta_1 I_3(q, \theta_1) (5 - 4 \sin^2 \theta_1) \sin^4 \theta_1. \quad (\text{E } 8)$$

Here, $I_3(q, \theta_1)$ is defined as the integral of $\exp[-q^4(\zeta_1^6 - 1)(\cos^4 \theta_1)/2]$ over $\zeta_1 = 1$ to ∞ . This integral is written in terms of the generalized exponential integral function, while the integration with respect to θ_1 in (E 8) yields an expression involving generalized hypergeometric functions, according to Mathematica (Wolfram Research). Here, we note that $q^7 I_3(q, \theta_1)$ tends to 0 as q approaches zero, and that $I_3(q, \theta_1)$ diverges, more slowly than $1/|\theta_1 - \pi/2|$, as θ_1 approaches $\pi/2$. We thus have $0 < \delta_e < 4.00 \times 10^{-2}\epsilon$.

REFERENCES

- ALLEGRA, J. C., STEIN, A. & ALLEN, G. F. 1971 Tracer diffusion and shear viscosity for the system isobutyric acid-water near the critical mixing point. *J. Chem. Phys.* **55**, 1716–1720.
- ANISIMOV, M. A., GORODETSKII, E. E., KLIKOV, D & SENGERS, J. V. 1995 Crossover between vapor-liquid and consolute critical phenomena. *Phys. Rev. E* **51**, 1199–1214.
- BARRERA, R. G., ESTÉVEZ, G. A. & GIRALDO, J. 1985 Vector spherical harmonics and their application to magnetostatics. *Eur. J. Phys.* **6**, 287–294.
- BEDEAUX, D. & MAZUR, P. 1974 Brownian motion and fluctuating hydrodynamics. *Physica* **76**, 247–258.
- BERG, R. F. & MOLDOVER, M. R. 1989 Critical exponent for the viscosity of four binary liquids. *J. Chem. Phys.* **89**, 3694–3704.

- BERG, R. F. & MOLDOVER, M. R. 1990 Critical exponent for viscosity. *Phys. Rev. A* **42**, 7183–7187.
- BEYSENS, D. 2019 Brownian motion in strongly fluctuating liquid. *Thermodyn. Interfaces Fluid Mech.* **3**, 1–8.
- BEYSENS, D., BOURGOU, A. & CALMETTES, P. 1985 Experimental determinations of universal amplitude combinations for binary fluids. I. Statics. *Phys. Rev. A* **26**, 3589–3609.
- BEYSENS, D. & ESTÈVE, D. 1985 Adsorption phenomena at the surface of silica spheres in a binary liquid mixture. *Phys. Rev. Lett.* **54**, 2123–2126.
- BEYSENS, D. & GBADAMASSI, M. 1980 Shear-induced effects on critical concentration fluctuations. *Phys. Rev. A* **22**, 2250–2261.
- BEYSENS, D., GBADAMASSI, M. & BOYER, L. 1979 Light-scattering study of a critical mixture with shear flow. *Phys. Rev. Lett.* **43**, 1253–1256.
- BEYSENS, D. & LEIBLER, S. 1982 Observation of an anomalous adsorption in a critical binary mixture. *J. Phys. Lett.* **43**, 133–136.
- BIAN, X., KIM, C. & KARNIADAKIS, G. 2016 111 years of Brownian motion. *Soft Matt.* **12**, 6331–6346.
- CHU, B., SCHOENES, F. J. & KAO, W. P. 1968 Spatial and time-dependent concentration fluctuations of the isobutyric acid-water system in the neighborhood of its critical mixing point. *J. Am. Chem. Soc.* **90** (12), 3042–3048.
- CLERKE, E. A. & SENGERS, J. V. 1983 Fast pressure quenches near the critical point of a binary liquid mixture. *Physica A* **118**, 360–370.
- EINSTEIN, A. 1905 On the motion of small particles suspended in liquids at rest required by the molecular-kinetic theory of heat. *Ann. Phys. (Leipzig)* **322**, 549–560.
- FOLK, R. & MOSER, G. 1998 Critical dynamics in mixtures. *Phys. Rev. E* **58**, 6246–6274.
- FOLK, R. & MOSER, G. 2006 Critical dynamics: a field-theoretical approach. *J. Phys. A: Math. Gen.* **39**, R207–R313.
- FUJITANI, Y. 2007 Connection of fields across the interface in the fluid particle dynamics method for colloidal dispersions. *J. Phys. Soc. Japan* **76**, 064401.
- FUJITANI, Y. 2018 Osmotic effects on dynamics of a colloidal rigid sphere in a near-critical binary fluid mixture. *J. Phys. Soc. Japan* **87**, 084602.
- FURUKAWA, A., GAMBASSI, A., DIETRICH, S. & TANAKA, H. 2013 Nonequilibrium critical casimir effect in binary fluids. *Phys. Rev. Lett.* **111**, 055701.
- HOHENBERG, P. C. & HALPERIN, B. I. 1977 Theory of dynamic critical phenomena. *Rev. Mod. Phys.* **49**, 435–479.
- KAWASAKI, K. 1970 Kinetic equations and time correlation functions of critical fluctuations. *Ann. Phys. (N.Y.)* **61**, 1–56.
- KEBLINSKI, P. & THOMIN, J. 2006 Hydrodynamic field around a Brownian particle. *Phys. Rev. E* **73**, 010502(R).
- KLIMONTOVICH, Y. 1994 Nonlinear Brownian motion. *Phys. Uspekhi* **37**, 737–767.
- LAMB, H. 1932 *Hydrodynamics*, 6th edn. Dover. § 92.
- LEE, S. P. 1976 Evidence for the “correlated layer” effect on the effective viscosity from Brownian motion in a ternary liquid mixture. *Phys. Rev. Lett.* **36**, 1319–1322.
- LINDNER, B. 2007 The diffusion coefficient of nonlinear Brownian motion. *New J. Phys.* **9**, 136.
- LORENTZ, H. A. 1896 A general theorem concerning the motion of a viscous fluid and a few consequences derived from it. *Versl. Kon. Akad. Wetensch. Amsterdam* **5**, 168–175.
- MAZUR, P. & VAN DER ZWAN, G. 1978 Brownian motion in a fluid close to its’ critical point. *Physica A* **92**, 483–500.
- MEHROTRA, A. K., MONNERY, W. D. & SVRCEK, W. Y. 1996 A review of practical calculation methods for the viscosity of liquid hydrocarbons and their mixtures. *Fluid Phase Equilib.* **117**, 344–355.
- MORSE, P. M. & FESHBACH, H. 1953 *Methods of Theoretical Physics*. Chap. 13. McGraw-Hill.
- OHTA, T. 1975 Selfconsistent calculation of dynamic critical exponents for classical liquid. *Prog. Theor. Phys.* **54**, 1566–1568.
- OHTA, T. & KAWASAKI, K. 1976 Mode coupling theory of dynamic critical phenomena for classical liquids. I: dynamic critical exponents. *Prog. Theor. Phys.* **55**, 1384–1395.
- OKAMOTO, R., FUJITANI, Y. & KOMURA, S. 2013 Drag coefficient of a rigid spherical particle in a near-critical binary fluid mixture. *J. Phys. Soc. Japan* **82**, 084003.

- OMARI, R. A., GRABOWSKI, C. A. & MUKHOPADHYAY, A. 2009 Effect of surface curvature on critical adsorption. *Phys. Rev. Lett.* **103**, 225705.
- ONUKEI, A. 2002 *Phase Transition Dynamics*. Cambridge University Press. § 2.3.5, § 6.1.3, § 6.2.1, and § 11.1.
- ONUKEI, A. & KAWASAKI, K. 1979 Nonequilibrium steady state of critical fluids under shear flow: a renormalization group approach. *Ann. Phys. (N.Y.)* **121**, 456–528.
- ONUKEI, A. & KAWASAKI, K. 1980a Critical phenomena of classical fluids under flow. I. *Prog. Theor. Phys.* **63**, 122–139.
- ONUKEI, A. & KAWASAKI, K. 1980b Non-Newtonian effect and normal stress effect in critical fluids. *Phys. Lett. A* **75**, 485–487.
- ONUKEI, A. & KAWASAKI, K. 1980c Critical phenomena in two-dimensional incompressible flow. *Prog. Theor. Phys. Suppl.* **69**, 146–159.
- ONUKEI, A., YAMAZAKI, K. & KAWASAKI, K. 1981 Light scattering by critical fluids under shear flow. *Ann. Phys. (N.Y.)* **131**, 217–242.
- OXTOBY, W. 1975 Shear gradient dependence of the viscosity of critical mixtures. *Phys. Lett. A* **50**, 459–460.
- PELISETTO, A. & VICARI, E. 2002 Critical phenomena and renormalization-group theory. *Phys. Rep.* **368**, 549–727.
- PÉREZ-SANCHEZ, G., LOSADA-PÉREZ, P., CERDEIRIÑA, C. A., SENGERS, J. V. & ANISIMOV, A. M. 2010 Asymmetric criticality in weakly compressible liquid mixtures. *J. Chem. Phys.* **132**, 154502.
- RALLISON, J. M. 1984 The deformation of small drops and bubbles in shear flows. *Annu. Rev. Fluid Mech.* **16**, 45–66.
- RISKEN, H. 2002 *The Fokker–Planck Equation*, 5th edn. Springer. § 3.3.3, § 5.2, and § S.9.
- SEKIMOTO, K. 2010 *Stochastic Energetics*. Springer. § 1.2.2 and § 1.3.2.
- SENGERS, J. V. 1985 Transport properties near critical points. *Intl J. Thermophys.* **6**, 203–232.
- SIGGIA, E. D., HOHENBERG, P. C. & HALPERIN, B. I. 1976 Renormalization-group treatment of the critical dynamics of the binary-fluid and gas-liquid transitions. *Phys. Rev. B* **13**, 2110–2123.
- STOKES, G. G. 1851 On the effect of the internal friction of fluids on the motion of pendulums. *Trans. Camb. Phil. Soc.* **9**, 8–106.
- SUTHERLAND, W. 1905 A dynamical theory of diffusion for non-electrolytes and the molecular mass of albumin. *Phil. Mag.* **9**, 781–785.
- SWINNEY, H. & HENRY, D. L. 1973 Dynamics of fluids near the critical point: decay rate of order-parameter fluctuations. *Phys. Rev. A* **8**, 2586–2617.
- TANI, H. & FUJITANI, Y. 2018 Drag coefficient of a circular inclusion in a near-critical binary fluid membrane drag coefficient of a circular inclusion in a near-critical binary fluid membrane. *J. Phys. Soc. Japan* **87**, 104601.
- TOUMI, A. & BOUANZ, M. 2008 Volumetric and refractive index properties of isobutyric acid-water binary mixtures at temperature ranging from 300.15 to 313.15 K. *J. Mol. Liquids* **139**, 55–60.
- YABUNAKA, S & FUJITANI, Y. 2020 Drag coefficient of a rigid spherical particle in a near-critical binary fluid mixture, beyond the regime of the Gaussian model. *J. Fluid Mech.* **886**, A2.
- ZWANZIG, R. & BIXON, M. 1975 Compressibility effects in the hydrodynamic theory of Brownian motion. *J. Fluid Mech.* **69**, 21.